INITIAL RESULTS FROM A LOW DENSITY, HYPERVELOCITY WIND TUNNEL

J. L. Potter,[1] M. Kinslow,[2] G. D. Arney Jr.[2] and A. B. Bailey[2]

ARO, Inc., Tullahoma, Tennessee

ABSTRACT

A small, low density, hypervelocity, continuous wind tunnel operating at total temperatures from 2000 to 4000 K is described briefly, and initial experiments designed to determine the characteristics of the flow are discussed. Effects of low Reynolds numbers on moderately cooled impact pressure probes and static pressure probes are shown. Preliminary work with a probe for measuring local mass-flow rate is outlined, and results are shown to be in agreement with impact and static pressure measurements. Axial and transverse surveys of flow in the nozzle are presented to illustrate the extent of boundary layer growth and the usable core of flow. A diffuser is proved to be advantageous, even though very low Reynolds numbers are typical of the tunnel. A comparison is presented of data on drag of spheres, including measurements from the new wind tunnel.

INTRODUCTION

Flight at altitudes greater than 40 miles above Earth, or at equal densities in atmospheres of other planets, generally is characterized by very low Reynolds numbers and high Mach numbers. In this regime, the flow around bodies is strongly affected by the viscous and compressible nature of the fluid medium, including mutual interaction of these and other real-gas attributes. Under the same conditions, pronounced thermal nonequilibrium is likely to further complicate matters.

Presented at ARS International Hypersonics Conference, Cambridge, Massachusetts, August 16-18, 1961; work reported herein was sponsored by the United States Air Force and conducted at the Arnold Center of the Air Force Systems Command.

[1]Manager, Research Branch, von Karman Gas Dynamics Facility.

[2]Engineer, Research Branch, von Karman Gas Dynamics Facility.

Aerodynamic forces, although possibly small, may be very important in the outer regions of planetary atmospheres because of critical flight maneuvers or effects on the subsequent path of the vehicle. Figure 1 illustrates this point by showing that significant aerodynamic forces may exist under conditions where there are major departures from the state of affairs characterized by thin boundary layers. The boundaries separating the various areas of low density phenomena have been defined by Probstein (Ref. 1). There is need for research on problems of low density hypervelocity flow, and experimental facilities should be welcome at this time if they provide trustworthy data applicable to any significant part of the problem.

The object of this paper is to report briefly on a small facility constructed at the Arnold Center of the Air Force Systems Command to explore the feasibility of continuous, arc heated wind tunnels for low density gasdynamics experiments. Because of the unusual flow conditions, calibration of the tunnel is particularly important, yet at the same time it is also more difficult. For these reasons, the main theme of this discussion is calibration, although brief descriptions of the wind tunnel and some diffuser research also are included. In this case, calibration includes work on flow probes as well as results of their use to survey the flow. Also, it includes comparative measurements of drag on simple shapes which may be compared with data from other sources.

DESCRIPTION OF WIND TUNNEL

A photograph of the wind tunnel is shown in Fig. 2. Restricted space around the tunnel prevented a more inclusive view, so the highly simplified sketch in Fig. 3 is included to supplement the photograph. The facility may be described as a continuous, arc heated, low density, hypervelocity or hypersonic, prototype wind tunnel. For convenience, it is referred to as the LDH Tunnel. It is continuous in the original sense, often operating for four or more hours without halting. Augmented cooling is by means of water forced through internal passages, and no unusual problems have been encountered in this respect. There is a significant loss of heating efficiency inherent with the need to cool fairly large areas in the plasma torch, settling chamber and nozzle. Overall heating efficiency varies between 10 and 15%, whereas the plasma torch alone has an efficiency approaching 60%. The arc heater is a 40-kw unit, but it normally operates at less than 20 kw with the present tunnel system. The LDH pumping system combines two stages of air injection with an existing vacuum pumping system built for some older, intermittent tunnels. It represents an effort to take advantage of available resources for the sake of economy. Al-

though largely made from cannibalized parts, it has proved very reliable and yields good performance.

The diameter at the exit of the hypersonic nozzle is 5.84 in. but boundary layer thickness reduces the useful core of uniform flow to approximately 1 in. under usual conditions. The latter feature arises, of course, from the very conditions intended to be created in the tunnel. The situation would be much worse if the benefits of a favorable wall heat transfer situation corresponding to $T_w/T_o \approx 1/10$ did not exist. Reservoir conditions and test section conditions are easily controlled and repeatable. The additional effort necessary to create high velocities and high stagnation temperatures is believed justified because it results in substantially closer simulation of free flight flow fields. This is important in regard to such aerodynamic phenomena as viscous interaction and the changes in fluid transport and thermal properties as the fluid is compressed and expanded in passing around a body.

Usual operating conditions with the original nozzle fall within the indicated ranges when computed for flow in thermal equilibrium.

Gas	N_2 (other gases may be used)
Total temperature	2000-4000 K
Total pressure	12-18 psia
Mach number	9-11
Velocity	7000-10,000 fps
Dynamic pressure	2-4 psf
Unit Reynolds number	220-420 per in.
Equivalent density altitude	50 miles (approx.)

In view of the low densities, high speeds and small size combined in this wind tunnel nozzle, there is a strong possibility of thermal nonequilibrium. On the basis of published reaction rates for nitrogen, both in regard to molecular vibration (Ref. 2) and dissociation (Ref. 3), it appears justifiable in the present case to assume equilibrium in the settling chamber just upstream of the nozzle. Then, since little or no dissociation should exist in the nozzle under ordinary operating conditions, one may assume thermal equilibrium throughout the nozzle and compute corresponding test section conditions. Comparison of these latter calculations with results based on a frozen process should furnish some feeling for the possible uncertainity in flow parameters. The following is an example of these calculations for typical (equilibrium) stagnation conditions of

3020 K and 17.79 psi in nitrogen. Basis of the comparison is $p_{\acute{o}}/p_o$ = constant in both flows.

	Equilibrium flow	Vibration frozen throughout
M	9.4	10.5
U	8690 fps	8270 fps
p	19.8 Hg	15.4 Hg
T	190 °K	143 °K
	3.9×10^{-5} atm	3.86×10^{-5} atm
q	3.50 psf	3.31 psf
Re	240 per in.	294 per in.

When the differences in the quantities expected to exert the greater influence on measured data are considered, it is apparent that evidence of vibrational nonequilibrium will be difficult to find. In this example, it is interesting to note that the Reynolds number of consequence in tests of blunt bodies, Re_2, is 47 per in. for equilibrium flow and 37 per in. for frozen flow. Where necessary in the remainder of this discussion, a distinction between equilibrium and frozen flows will be made. Unless stated otherwise, any flow parameters used later will be based on thermal equilibrium.

A photograph of a blunt model, similar to a Mercury capsule, installed in the LDH Tunnel is shown in Fig. 4. Flow visualization has been achieved by creating an electric field around the model through the mechanism of a difference in potential maintained by a Tesla coil. A more complete description of this wind tunnel is given in an Arnold Center report (Ref. 4).

RESULTS FROM INITIAL EXPERIMENTS

The high temperatures encountered in this tunnel make it necessary to determine total enthalpy partially by indirect means. There is the possibility of energy losses between settling chamber and test section caused by viscous shear and heat transfer. This, as well as the question of thermodynamic equilibrium mentioned earlier, makes it particularly desirable to collect as many independent calibration data as possible. The most valuable data are those giving test section conditions directly. In fact, if techniques for doing this were developed to a reliable state, the calibration of all types of high enthalpy tunnels would be far less dependent on assumptions and theoretical estimates.

It should be recognized that most of the flow probing procedures commonly used in higher density, lower speed flows are not directly or easily applicable in low density, hypervelocity

streams. In this class fall static pressure probes, total temperature probes, and shock angle or Mach line photography. Therefore, the authors have spent much time conducting and evaluating results from various calibration experiments designed to circumvent or at least account for viscous and thermal effects. Results of this work, in some cases preliminary in nature, are described in the following sections.

IMPACT PRESSURE PROBES

The impact pressure or pitot probe deserves its place at the top of this list because of its simplicity, the usually straightforward interpretation of its readings, and most certainly because of its widespread use. Indeed, calculated flow parameters based on an impact pressure and assumed equilibrium or frozen isentropic expansion from partly measured and partly computed reservoir conditions often are considered sufficient tunnel calibration. First surveys of the LDH Tunnel nozzle were made by impact pressure probes, but the verification of those results by independent measurements has been a goal.

After the time-consuming preparatory work directed toward simultaneous improvement of the tunnel and instrumentation as well as preliminary definition of flow conditions, a series of experiments was begun to establish the accuracy of the impact pressure data. Two fundamental problems requiring attention were: possible error caused by large thermal gradient along the probe; and possible error arising from a viscous effect at the probe mouth. The first of these is discussed by Dushman (Ref. 5), Kennard (Ref. 6), and others. Howard (Ref. 7) has published useful experimental data. The second has been the subject of several investigations, particularly at the Universities of California and Toronto, for example, Sherman (Ref. 8), Chambre and Schaaf (Ref. 9) and Enkenhus (Ref. 10).

The error due to temperature gradient also is a function of pressure level or Knudsen number. Inasmuch as typical impact pressures in the LDH Tunnel are in the range from 1500 to 3000 μ Hg, the effect of temperature gradient on impact pressure measurements is slight when using a water cooled probe having a bore diam of approximately 0.1 in. or greater. This has been established by experiments and is in agreement with the data of Ref. 7. Therefore, calibration surveys of the LDH Tunnel nozzle customarily are made with such a probe. The thermal gradient correction is appreciable for very small impact probes or static pressure probes.

Shape of the head of the probe is a factor in determining the viscous effect; and because it was considered more convenient to

use flat faced probes in the LDH Tunnel, an investigation was conducted to establish the Reynolds number at which such influence is manifest. A summary of the earlier results is included in Fig. 5, where some data from other sources also are compared. It will be noted that all measurements involving the flat faced, or nearly flat faced, chamfered probes show highly satisfactory agreement, although the LDH Tunnel results correspond to a markedly higher Mach number and a moderately cooled wall condition of $T_w/T_o \approx 1/4$, compared with the other data for which $T_w/T_o \approx 1$. The ratio $T_w/T_o \approx 1/4$ could have been reduced by more elaborate cooling, but that was not thought to be necessary in this case. The approximate correction of the LDH experimental data to account for the temperature gradient along the probe does not produce a significant change in the results, except at the lower Reynolds numbers.

STATIC PRESSURE PROBES

Measurement of free stream static pressure in the LDH Tunnel is difficult because the very thick boundary layer on a conventional probe creates a spuriously high pressure at orifices located any practical distance from the stagnation point. Static pressure may be found by means of nozzle wall orifices, but there would be much doubt regarding radial pressure gradients associated with nozzles having large rates of increase of cross-sectional area and very thick boundary layers. Therefore, some exploratory measurements have been made using a family of probes having conical noses and cylindrical afterbodies with orifice locations at varying distances downstream of the stagnation points. In doing this it was hoped that the pressure in the free stream could be found by extrapolating the pressure distribution along the probe to the limit of infinite length. Realizing the perils of extrapolation processes, as well as other sources of possible error, the result was not regarded as infallible. On the other hand, free stream static pressure is a useful supplement to other measurements which, taken all together, lead to sure definition of the flow conditions.

Keeping in mind the thick boundary layer on the probes, it is assumed that the pressure distribution is determined largely by the displacement thickness. Where the growth of the displacement thickness is rapid, as it is at the orifice locations, pressure will be approximately proportional to the reciprocal of distance from the stagnation point x. As $x \to \infty$, the rate of change of p with $1/x$ will decrease. Therefore, the authors have chosen to plot static pressure against a parameter which contains x in the denominator, since the resulting curve should be linear throughout the region where most of the data points appear.

There is an axial Mach number gradient of 0.14 per in. for a typical case in the original conical nozzle which has remained in use to the present time. Because their small size made it practical to measure pressure at only one distance from the tip on each probe, the probe tips were located at different axial stations in the nozzle while data were taken at a fixed nozzle station. In other words, a number of probes were used to get the pressure distribution, rather than a single probe with many orifices. Therefore, the Mach number and the pressure distributions on the forward portions of the probes varied slightly from probe to probe. Assuming pressures all along a probe were determined entirely by Mach number and pressure at the probe stagnation point, it is estimated that the axial gradient in the nozzle would cause static pressures measured with the minimum value of $1/x$ to be approximately 1.3-μ Hg high in relation to the pressure measured with the largest value of $1/x$. However, since this estimate did not include consideration of the nozzle free stream gradient on boundary layer growth, it probably is safe to conclude that the net effect amounted to less than 1 Hg. Since differences of that magnitude could be concealed in the experimental error, no correction is applied to the measured data. It is intended that additional study of static pressure measurements will be taken up when the new contoured nozzle is installed. Then, it is hoped, the axial gradient will not exist.

Another and even more important factor affecting the results is the correction to each probe reading necessitated by the high Knudsen numbers in the probes and the temperature gradients along the probes. Although this was not significant in the impact pressure measurements, it is responsible for 20 to 40% corrective increases added to the measured static pressures. In this case, the data of Howard (Ref. 7) have been used. Additional research on the effect of temperature gradient on measurement of very low pressures is being conducted.

Figure 6 shows three pressure distributions determined by the described method. Pending elimination of the axial pressure gradient in the nozzle and more exact determination of the effect of thermal gradient along the probe, a detailed discussion of these data is not justified. However, the results appear reasonably promising. The two upper curves presumably should coincide. Since they do not, it may be assumed that inexact compensation for thermal gradient, nozzle pressure gradient or differences in orifice geometry may be the underlying cause. When the data are extrapolated as shown, the endpoints fall between the equilibrium and wholly frozen flow pressures based on impact pressure readings and assumed isentropic expansion from the settling chamber, that is, p_o'/p_o . These are denoted

by the thicker black bars on the ordinate, the tops of the bars representing thermal equilibrium and the bottom representing frozen vibrational modes throughout the system. Inasmuch as it is expected that the extrapolations should tend to level off as $1/x \to 0$, the true static pressures in both cases appear to be close to the equilibrium values. Unfortunately, the corrections for thermal gradient are so large that the data cannot be relied on to the degree necessary to prove or disprove thermal equilibrium. Even so, these results are valuable since they point to the existence of isentropic flow in the nozzle. Another point possibly deserving notice is decrease in pressures on the smaller probe at the smaller values of x (0.25 in.). Conceivably this could represent slip flow since $(M/\sqrt{Re_x}) = 1.2$ at this station.

Lateral traversing of a probe has shown constant static pressure across the core of uniform flow at the exit of the LDH Tunnel. When a tubular extension of 5.84 in. inside diam is connected to the nozzle exit so that the conical nozzle is followed by about 12 in. of constant area duct, the higher tank pressure cannot make its influence felt upstream through the subsonic portion of the boundary layer. Then, an investigation with $T_o = 3020$ K shows that static pressure computed from centerline impact pressure ratio p'/p_o and based on thermal equilibrium closely agrees with static pressure taken from an orifice in the wall of the nozzle at the corresponding axial station.

MASS FLOW PROBE

As part of the extended calibration program demanded by the low density, hypervelocity character of the nozzle flow, a mass flow probe was tested. The idea certainly is not new, but successful application seems to be rare. There are several points at which failure may occur in attempting to measure local mass-rate-of-flow, but the possibility of deriving valuable data from the experiment encouraged the present effort. Obviously, if the product $(\rho U)_\infty$ can be measured by a mass flow probe, this can be compared to the value computed on the basis of impact pressure measurements, and agreement would constitute strong proof of the accuracy of all other calibration data based on isentropic nozzle flow. Also, since in hypersonic flow impact pressure $p' \approx (\rho U^2)$, one may obtain ρ_∞ and U_∞ directly from impact-pressure and mass-flow probe measurements.

A schematic diagram of the equipment used is shown in Fig. 7, and the sequence of operation follows:

1) The probe tip is positioned at the point where the local quantity $(\rho U)_\infty$ is to be measured.

2) Ideally, with valves 1, 3 and 6 open, the flow in a stream tube equal in area to the probe opening is swallowed into the probe. (Valves 2, 4 and 5 initially are closed.)

3) Valves 4 and 5 are manipulated in order to position the oil levels at A--A′, and are then left closed.

4) Needle valve 6 is adjusted so that the pressure above the oil level at A is increased to a conveniently measurable value, but is still low enough to ensure that the flow ahead of the probe tip is swallowed.

5) The pressure at the micromanometer and the oil height in the sight glass are noted.

6) Valve 3 is closed simultaneously with the opening of valve 4, and the time is noted. The oil level then begins to drop, providing space for the mass flow from the probe.

7) Valve 4 is closed so that the oil level will stabilize at levels B--B′. The pressure above the oil is now less than the initial pressure due to the increased volume. The pressure is increasing because of the incoming flow.

8) When the pressure indicated on the micromanometer is the same as that noted in step 5, valve 1 is closed, valve 2 is opened, and the time is noted again.

9) The mass flow through the probe is given by

$$\dot{m}_1 = \rho_v \Delta V/\Delta t \qquad (1)$$

If $\dot{m}_1 = (\rho U)_\infty A_p$

then $$(\rho U)_\infty = \rho_v \Delta V/(A_p \Delta t) \qquad (2)$$

Also feasible is a second approach wherein the oil is omitted and the tank merely allowed to rise from a very low initial pressure to some limiting higher pressure as mass is passed into it. Of course, it must be determined that mass-flow-rate is not variable with pressure during this process.

The most crucial factor in this experimental procedure is the swallowing of the shock wave at the probe inlet. If the shock is not swallowed, effective inlet area is not equal to geometric area, and the measurement is useless unless some

form of calibration can be devised. Using the type of equipment described herein, one could plot local mass-flow-rate as a function of p_v and find a value of p_v below which $\dot{m}_1$ becomes constant. In practice, however, the combination of limited tank size and narrow usable range of p_v's prevented full application of this checking technique. The system is being improved so that more thorough investigations can be made. Investigation indicates that the shock was nearly, but not completely, swallowed when the probe inlet was near the nozzle exit. Complete swallowing is believed to have been accomplished upstream of X = -3 for T_o = 3020K and upstream of X = -5 for T_o = 2220K. Results of the first measurements are presented in Fig. 8.

Calculated $(\rho U)_\infty$, based on isentropic expansion and measured p_o'/p_o, also are shown in Fig. 8 for comparison with the direct measurements of $(\rho U)_\infty$. Considering the experimental difficulties and accuracy of both types of data, the agreement is very encouraging.

NOZZLE FLOW SURVEYS

Design of the first nozzle for this wind tunnel was based on less secure grounds than present-day design of nozzles for more conventional tunnels. In the first place, the very conditions intended to be produced made the boundary layer growth and viscous losses dominant in determining both nozzle contour and required pressure ratio. Second, performance of the pumping system was based entirely on calculated jet-ejector performance, so the relation between flow rate and tunnel end pressure was not known with certainty. Last, it was planned to operate continuously with very high stagnation temperatures, which made design of the nozzle cooling system important. The fact that the original nozzle proved almost ideal attests to the good fortune attending these estimates.

The nozzle is conical, expanding from a throat diam of 0.102 in. to an exit of 5.84 in. with a 30-deg included angle. The conical expansion was adopted on the basis of estimated performance of other tunnel components and estimates of boundary layer growth for expected nozzle Mach and Reynolds numbers. Since these estimates indicated an approximately conical shape, the obvious machining ease decided the issue. Results of typical transverse impact pressure and relative total temperature surveys in the original nozzle are shown in Fig. 9. The so-called relative total temperature was obtained using a conventional, singlyshielded, total temperature probe of the type often used in unheated supersonic flows. Thus, a greater part of the heat transmitted to the probe was lost through conduction

and radiation, making the thermocouple output suitable only to indicate lateral distribution of heat flux at a given axial station in the nozzle. However, this information is valuable as a supplement to impact pressure profiles. Aside from the effect of low Reynolds number on impact pressure probes, there is the well-known difficulty with impact pressure probes in regions where large lateral gradients in Mach number and other quantities exist. Such conditions are typical of the edges of hypersonic boundary layers. Thus, even a merely relative total temperature may be more indicative of flow conditions at the edge of the core of uniform flow in the nozzle.

Figure 9 reveals that the tremendous boundary layer growth materialized as expected, showing that test section size of such wind tunnels really must be quoted in terms of "core diameter" to be meaningful. To take full advantage of the present rather marginal pumping performance, the nozzle is designed to overexpand. Thus, a weak, reversed conical shock emanates from near the exit of the nozzle. In a typical case this shock raises static pressure from about 15 μHg ahead of the shock to roughly 60 μHg downstream, thereby balancing pressure along the border of the hypersonic jet between nozzle exit and diffuser entrance. This is seen in Fig. 10, which shows three typical axial impact-pressure surveys. Location of the trailing shock depends on operating conditions, such as diffuser position and model blockage. Its position often is made visible by the increased heating and red coloration locally on a sting or probe extending from the test section back through the shock.

The boundary layer in this nozzle has a typical laminar hypersonic profile and is developed in the presence of a favorable wall heat transfer condition, with T_x/T_o approximately one-tenth. The throat of the present nozzle remains relatively cool during tunnel operation. In a typical situation, with stagnation pressure 17.79 psia, stagnation temperature 302°K and 3.6 lb/hr nitrogen flow rate, the entire nozzle cooling loss amounts to slightly over 20% of the total input power to the heater.

DIFFUSER INVESTIGATIONS

A diffuser is a rather unusual component for a low density wind tunnel. Because of the very pronounced viscous losses corresponding to the low Reynolds numbers throughout these tunnels, pressure recovery is poor and usually not especially attempted. However, even a small degree of recovery is valuable, and it was believed that some effort toward that end would be worthwhile. Therefore, the tunnel was designed so that various diffusers could be easily installed.

The first series of diffusers tested is described by Fig. 11. Design was rather arbitrary because of the absence of data for the combined low density, hypervelocity flow conditions. As an economy measure, one entrance cone, one exit cone and a series of central sections of varying diameters were fabricated from sheet metal. Starting with the smaller diam central section having greatest axial length, each succeeding configuration of equal minimum diam was made by cutting off part of the center section. Each succeeding diffuser of larger throat diam was made by cutting off part of the conical sections so that their smaller diameters matched the new central section. Thus, the effect of center section length was investigated with entrance and exit section lengths constant for any given throat diam, but the conical pieces became successively shorter with each increase in throat diam.

Inasmuch as tank static pressure rather than tunnel pressure ratio was of direct concern in the present case, results are presented in terms of the tank pressure. These are given in Fig. 12. Examination reveals that variation of axial length of the constant area diffuser throats had negligible effect on tank pressure. However, diameter of this throat section is quite important. The apparent optimum value of unity for the ratio of nozzle exit and diffuser throat diams probably is coincidental since much of the nozzle exit is filled with boundary layer. Free jet length was a factor in these tests, but it became less critical as the throat diam was enlarged. When the latter dimension exceeded the optimum, influence of free jet length became relatively unimportant.

It is interesting to review the contributions of various segments of the diffusers. Figure 13 shows that a simple short tube orifice in a wall reduced tank pressure from 60 to 30 μ Hg. Addition of a collector or convergent section further reduced tank pressure to 12 μHg. Completion of the diffuser by addition of the divergent section did not provide much additional benefit except when greater free jet lengths existed. It may also be noted that provision for a finite length of constant diam throat resulted in an improvement over the performance of a convergent cone-frustum alone.

Rise in tank pressure resulting from blockage decreased as diffuser throat diam increased. The small size of the tunnel makes it important to minimize the size of supporting struts and other obstacles in the stream. The influence of tank pressure on position of the nozzle shock is indicated in Fig. 14. Benefits of the diffuser may be appreciated when it is realized that the axial spread of shock positions in Fig. 14 covers approximately six useful test section diams. A more extensive

investigation of diffuser performance may be conducted in the future, but it is considered that the major gain already has been realized.

MEASUREMENTS OF DRAG OF SPHERES

In earlier days, sphere drag was used as a wind tunnel calibration test for determining stream turbulence. Sphere drag measurements have also gained an established place in low density wind tunnel work. In this connection, such data serve to extend knowledge of aerodynamic drag and also aid in tunnel calibration by enabling comparison of data taken from various tunnels. A limited series of measurements has been completed using the LDH Tunnel.

A water cooled, axial-force balance permitting measurement of loads in the range of 0.002-0.015 lb was used. This balance was built for another purpose and was used for the measurement of sphere drag because of its availability. As a result, the range of measurements was limited but nonetheless useful. The spheres were of solid steel and were maintained at surface temperatures T_w approximately equal to 0.3 total temperature T_o. Mach number was 9.4 and unit Reynolds number was 240 per in.

To compare data from various sources, a means of approximate correlation was attempted. If drag coefficients are plotted against a form of Reynolds number, such as Re_2, data obtained from tests in hypervelocity streams with $T_w \approx T_o$ will not agree with data from tests where $T_w \quad T_o$ and M 5. This is so because both the drag coefficients C_{Dc} at high Reynolds numbers, and the free molecular flow drag coefficients C_{Dfm} will be different. This obstacle to the comparison of data is largely eliminated by using the quantity $(C_D - C_{Dc})/(C_{Dfm} - C_{Dc})$ as the dependent variable. When presented in this form, variations in C_D due to differences in Mach numbers, temperatures and heat transfer tend to vanish. The data of Hodges (Ref. 11) may be used to obtain C_{Dc}. As a convenience, the faired data curve from Ref. 11 is reproduced here in Fig. 15. The free molecular drag coefficient for spheres, assuming completely diffuse reflection of incident molecules is given in Ref. 12 as

$$C_{Dfm} = \frac{\exp\frac{-S^2}{2}}{S^3\sqrt{\pi}}\,(1 + 2S^2) + \frac{4S^4 + 4S^2 - 1}{2S^4}\,\mathrm{erf}(S) + \frac{2\sqrt{\pi}}{3S_w} \qquad (3)$$

where $S = U_\infty / \sqrt{2RT_\infty}$ (4)

$$S_w = U_\infty / \sqrt{2RT_w} \quad (5)$$

Following this procedure, Fig. 16 has been prepared. In this case

$$Re_2 = (U/\nu)_2 D \quad (6)$$

and all quantities pertaining to the LDH Tunnel are based on flow in thermodynamic equilibrium. Inspection of the result leads to the conclusion that data from the LDH Tunnel are consistent with other published measurements. This tends to substantiate the nozzle calibration based on surveys with probes discussed previously and demonstrates that useful aerodynamic data are obtainable with this facility.

CONCLUSIONS

1) Preliminary investigation at total temperature levels of 2000 to 4000K indicates that the arc heated, continuous, low density wind tunnel provides a useful testing environment for relatively precise and detailed experiments.

2) Development of calibration techniques enabling independent determinations of test section flow properties appears to be progressing satisfactorily. Data gathered thus far are self-consistent, repeatable and consistently point to the conclusion that an isentropic core exists in the nozzle. Evidence concerning thermal equilibrium is not so clear, possibly because only molecular vibration is involved and the influence is difficult to distinguish in a flow that is characterized by an unusual combination of low density and high speed.

3) Efforts to improve the pressure ratio across the nozzle through use of a diffuser were successful.

4) Comparison of the drag of spheres measured in the new tunnel and in other facilities is made easier by a normalization procedure defined in the discussion. Based on this correlation, it is concluded that the new data are valid and serve to support the tunnel calibration surveys using flow probes.

ACKNOWLEDGMENT

The valuable assistance of others associated with the low density wind tunnel project is recognized by the authors. In particular, David Boylan has participated in all of the

work reported, and Francis Armstrong and Mrs. Betty Majors have assisted with various phases.

NOMENCLATURE

A = cross-sectional area or reference area

C_D = drag coefficient

C_F = force coefficient, either lift or drag

D = reference diam, usually maximum

d = orifice or inside diam

h = height of manometer or gage fluid column

M = Mach number

$\dot{m}$ = mass-flow rate

p = pressure

q = dynamic pressure, $\rho U^2/2$

R = gas constant

r = body or nose radius

S = molecular speed ratio

T = temperature

t = time

U = velocity

V = volume

X = axial station is nozzle, zero at exit, positive downstream

X = axial length along probe, zero at stagnation point

Y = radial station in nozzle, zero on centerline, positive downward

γ = ratio of specific heats

μ = microns or 0.001 mm

γ = kinematic viscosity

ρ = density

Subscripts

a = dimensions of probe orifice

c = continuum, high Reynolds number condition

fm = free molecular flow condition

i = probe or tube inside diam

o = stagnation condition (total or reservoir). When used in combination with a prime, i.e., p_o , refers to conditions at stagnation point.

p = condition at inlet to mass-flow probe

∞ = free stream condition

1 = local value of a quantity

2 = condition immediately downstream of a normal shock wave

t = condition in tank surrounding tunnel nozzle and jet

v = condition inside mass-flow collecting tank

w = body surface or wall condition

x = based on the distance x

REFERENCES

1 Probstein, R. F., "Shock Wave and Flow Field Development in Hypersonic Re-Entry," presented at ARS Semi-Annual Meeting, Los Angeles, Calif., May 9-12, 1960 **,Preprint 1110-60.**

2 Blackman, V., "Vibrational Relaxation in Oxygen and Nitrogen," J. Fluid Mech., vol. 1, pt. 1, May 1956, pp. 61-85.

3 Wray, K., Teare, J. D., Kivel, B. and Hammerling, P., "Relaxation Processes and Reaction Rates Behind Shock Fronts in Air and Component Gases," Avco Research Lab., Research Rep. 83, Dec. 1959.

4 Potter, J. L., Kinslow, M., Arney, G. D., Jr. and Bailey, A. B., "Description and Preliminary Calibration of a Low-Density, Hypervelocity Wind Tunnel," AEDC-TN-61-83, Aug. 1961.

5 Dushman, S., "Scientific Foundations of Vacuum Technique," John Wiley and Sons, Inc., N. Y., 1949, pp. 65- 7.

6 Kennard, E. H., "Kinetic Theory of Gases," McGraw-Hill Book Co., Inc., N. Y., 1938, pp. 327-333.

7 Howard, W. M., "The Effect of Temperature on Pressures Measured in a Hypersonic Wind Tunnel, "J. Aero/Space Sci.," vol. 26 no. 11, Nov. 1959, p. 764.

8 Sherman, F. S., "New Experiments on Impact Pressure Interpretation in Supersonic and Subsonic Rarefield Air Streams," Univ. of California Instit. Engrg., Research Rep. no. He-150-99, Dec. 21, 1951.

9 Chambre, P. L. and Schaaf, S. A., "The Impact Tube," in "Physical Measurements in Gas Dynamics and Combustion," Princeton University Press, N. J., 1954, pp. 111-123.

10 Enkenhus, K. R., "Pressure Probes at Very Low Density," Univ. of Toronto, Instit. Aerophysics, UTIA Rep. no. 43, Jan. 1957.

11 Hodges, A. J., "The Drag Coefficient of Very High Velocity Spheres," J. Aero. Sci., vol. 24, no. 10, Oct. 1957, pp. 755-758.

12 Schaaf, S. A. and Chambre, P. L., "Flow of Rarefied Gases," in "Fundamentals of Gas Dynamics," Princeton University Press, N. J., 1958, p. 704.

13 Kane, E. D., "Drag Forces on Spheres in Low Density Supersonic Gas Flow," Univ. of California Instit. Engrg., Research Rep. no. HE-150-65, Feb. 15, 1950.

14 Sreekanth, A. K., "Aerodynamic Force Measurements in a Highly Rarefied Gas Stream," Bulletin and Annual Progress Report 1960, Univ. of Toronto, Instit. Aerophysics, Oct. 1960, pp. 12, 69, 70.

15 Wegener, P. P. and Ashkenas, "Wind Tunnel Measurements of Sphere Drag at Supersonic Speeds and Low Reynolds Numbers," Jet Propulsion Lab., California Inst. Tech., Tech. Release no 34-160, Nov. 25, 1960.

16 Masson, D. F., Morris, D. N. and Bloxsom, D. E., "Measurements of Sphere Drag from Hypersonic Continuum to Free Molecular Flow," Rand Corp. Research Memo. RM-2678, Nov. 3, 1960.

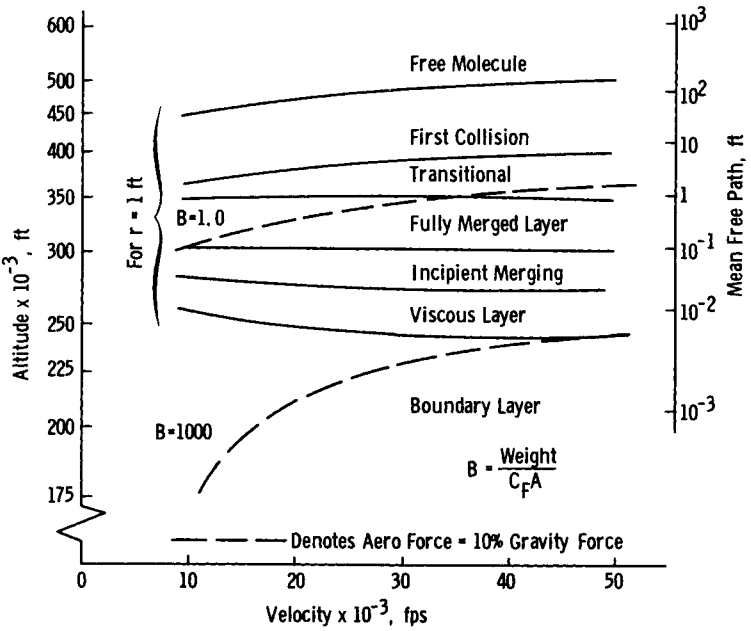

Fig. 1 Regimes of low density, hypervelocity flow defined for the stagnation region of a blunt, cooled body in Earth's atmosphere (see Ref. 1).

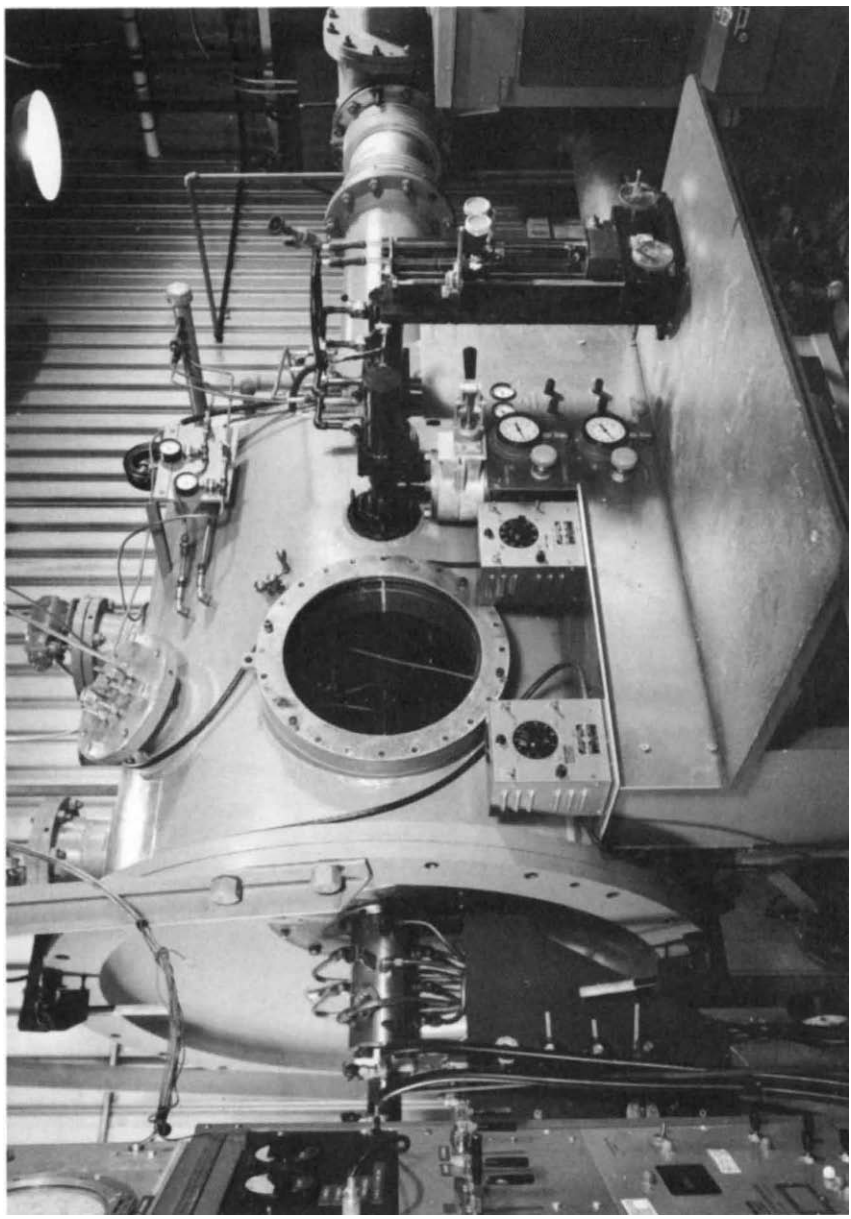

Fig. 2 Low density, hypervelocity (LDH) wind tunnel of the von Karman Gas Dynamics Facility, USAF Arnold Center.

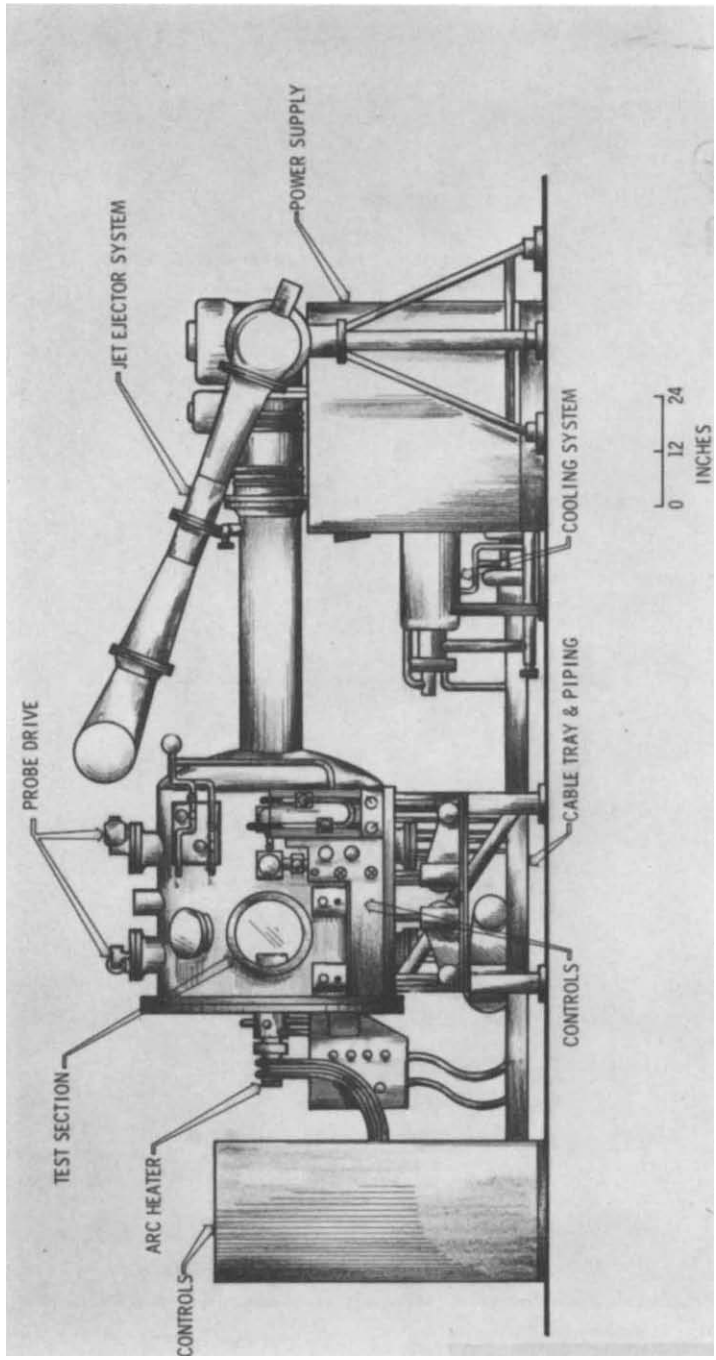

Fig. 3 Elevation view of the LDH wind tunnel with major components identified.

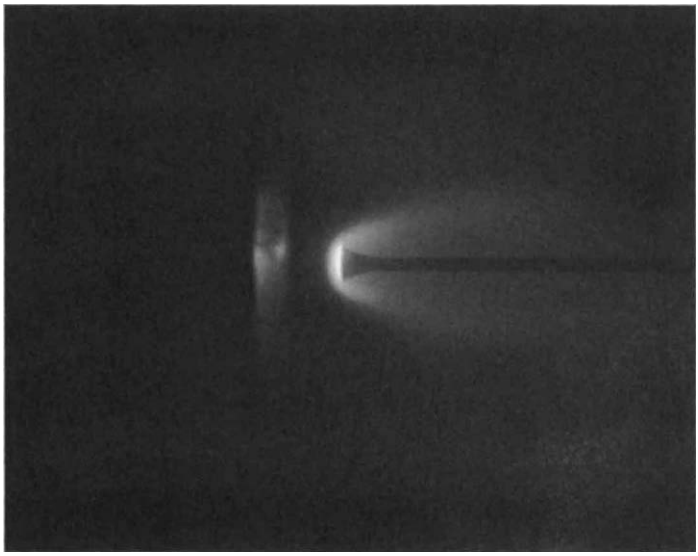

Fig. 4 Flow visualization produced by artificially created electric field; $M_\infty = 9.7$, $U_\infty = 8700$ fps, equivaler altitude = 50 miles.

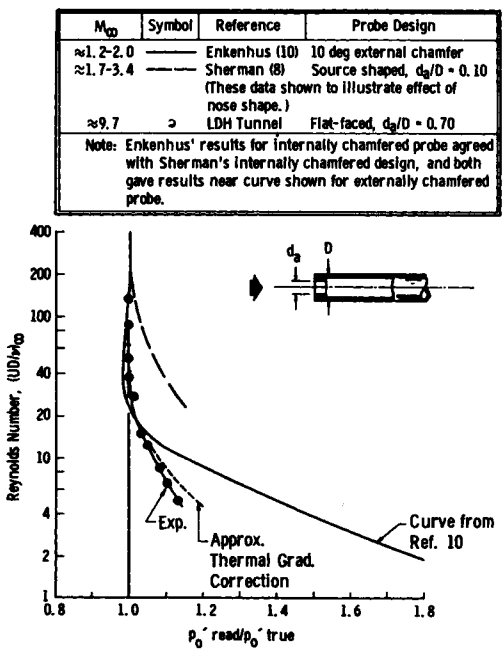

Fig. 5 Viscosity effect on readings of impact pressure probes at low Reynolds numbers and supersonic speeds.

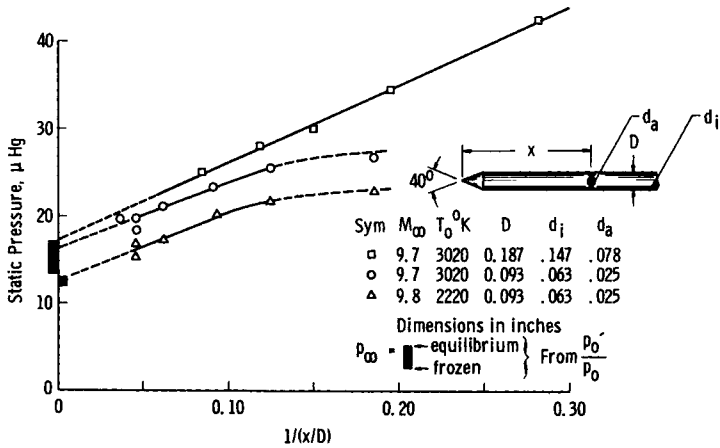

Fig. 6 Approximate determination of static pressure (data have been corrected for temperature gradient along the probe following Ref. 7).

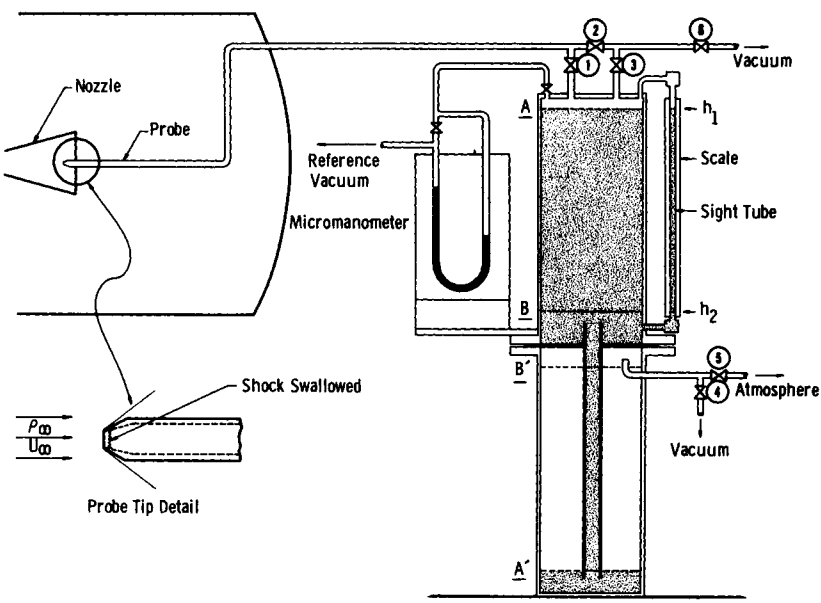

Fig. 7 Diagram of mass flow probe system.

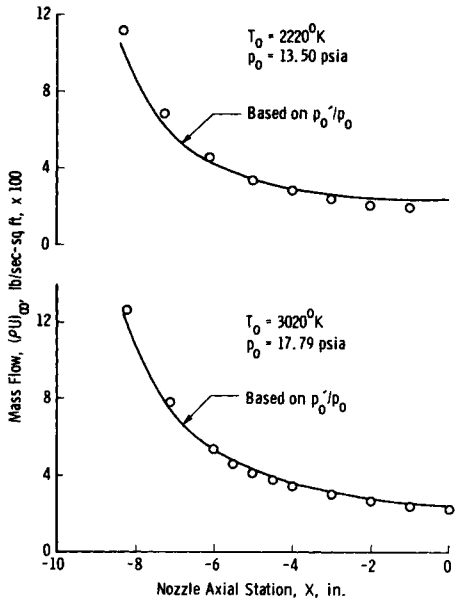

Fig. 8 Measurements with a mass flow probe (points represent local values on nozzle ℄).

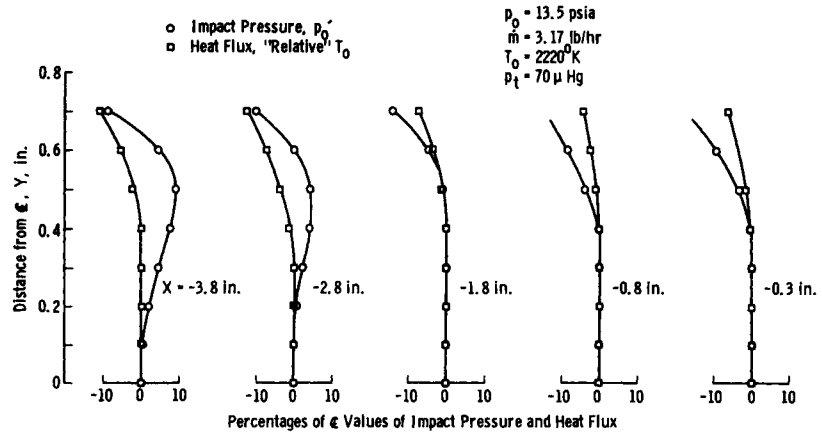

Fig. 9 Typical results of transverse surveys at various axial stations in the LDH tunnel conical nozzle (total angle = 30 deg).

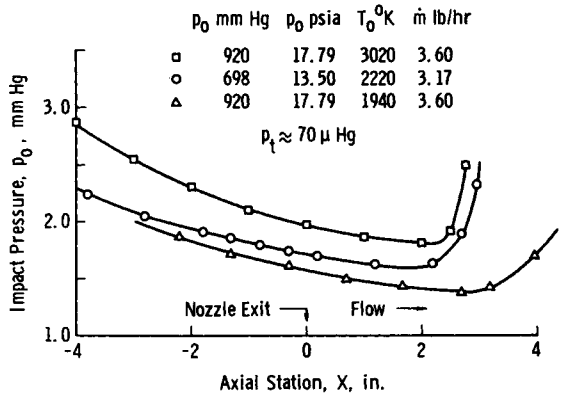

Fig. 10 Axial, centerline impact pressure distributions.

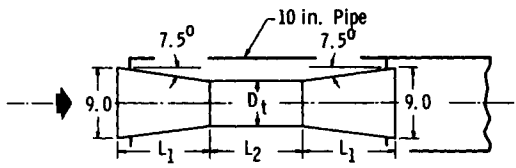

Dimensions in inches and degrees

Diffuser	L_1	L_2	D_t	Notes
1A	15	24	4.8	
1B	15	13.25	4.8	
1C	15	8.25	4.8	
2A	14	23.5	5.2	
2B	14	14	5.2	
2C	14	6	5.2	
3A	13	23.3	5.6	
3B	13	13.3	5.6	
3C	13	5	5.6	
4A	10.5	0	6	Convergent section only
4B	10.5	6	6	Convergent and throat sections
4C	0	6	6	Throat section only
4D	10.5	5.5	6	Complete diffuser
5A	9	5.875	6.375	

Fig. 11 Diffuser configurations.

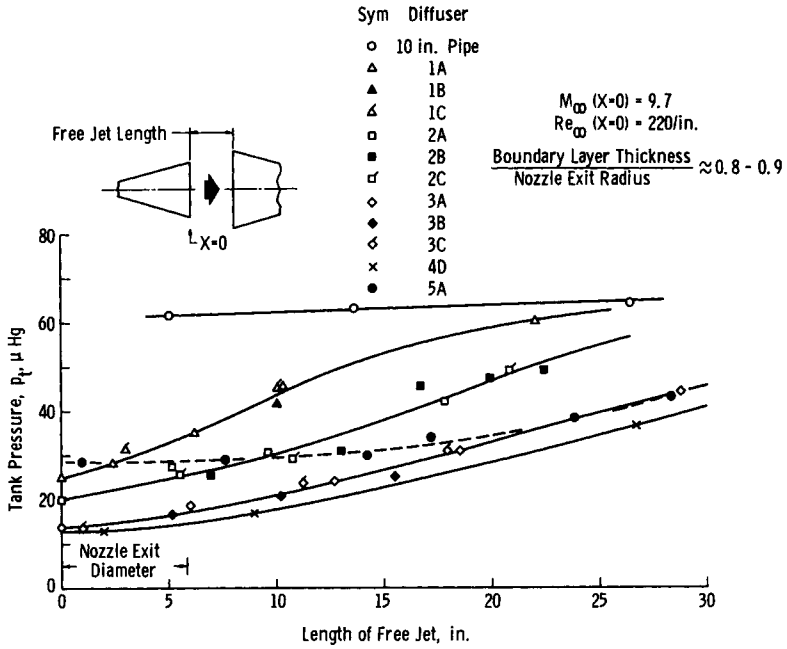

Fig. 12 Diffuser performance with clear jet.

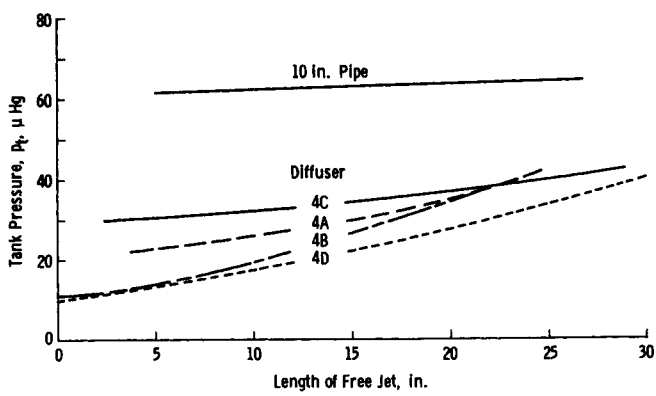

Fig. 13 Diffuser component contributions with clear jet.

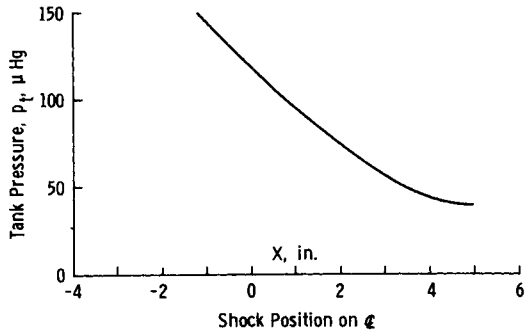

Fig. 14 Effect of tank pressure on shock position.

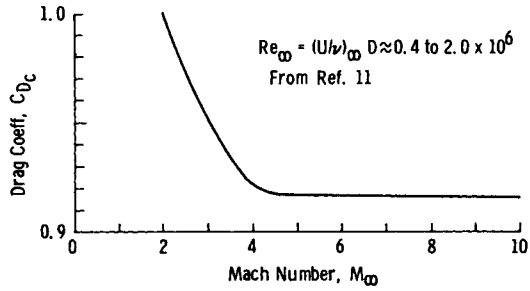

Fig. 15 Drag of spheres at high Reynolds and Mach numbers.

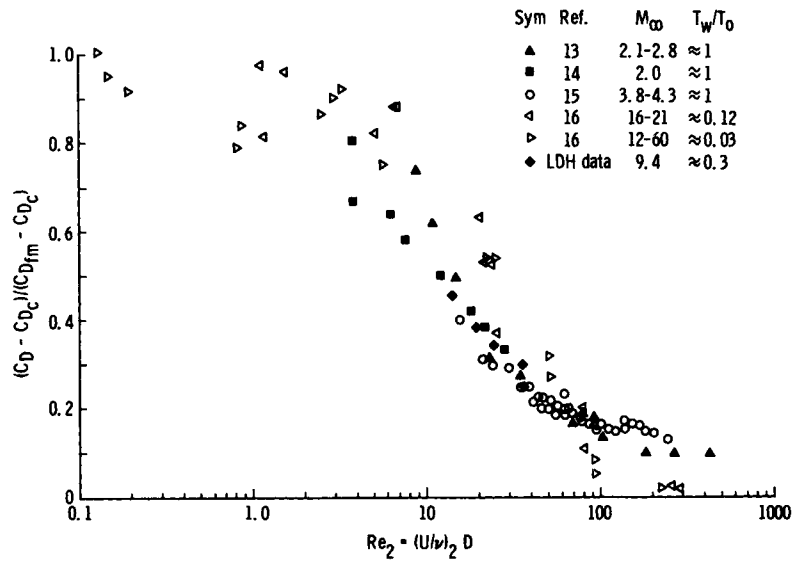

Fig. 16 Comparison of drag coefficients of spheres measured in low density wind tunnels.